THE JOURNAL OF PHYSICAL CHEMISTRY LETTERS
A JOURNAL OF THE AMERICAN CHEMICAL SOCIETY

pubs.acs.org/JPCL Letter

Quantum Tunneling in Reactions Modulated by External Electric Fields: Reactivity and Selectivity

Zhifeng Ma,[‡] Zeyin Yan,[‡] Xin Li,* and Lung Wa Chung*

Cite This: *J. Phys. Chem. Lett.* 2023, 14, 1124−1132 Read Online

ACCESS | Metrics & More | Article Recommendations | Supporting Information

ABSTRACT: Quantum tunneling and external electric fields (EEFs) can promote some reactions. However, the synergetic effect of an EEF on a tunneling-involving reaction and its temperature-dependence is not very clear. In this study, we extensively investigated how EEFs affect three reactions that involve hydrogen- or (ground- and excited-state) carbon-tunneling using reliable DFT, DLPNO−CCSD(T1), and variational transition-state theory methods. Our study revealed that oriented EEFs can significantly reduce the barrier and corresponding barrier width (and *vice versa*) through more electrostatic stabilization in transition states. These EEF effects enhance the nontunneling and tunneling-involving rates. Such EEF effects also decrease the crossover temperatures and quantum tunneling contribution, albeit with lower and thinner barriers. Moreover, EEFs can modulate and switch on/off the tunneling-driven 1,2-H migration of hydroxycarbenes under cryogenic conditions. Furthermore, our study predicts for the first time that EEF/tunneling synergy can control the chemo- or site-selectivity of one molecule bearing two similar/same reactive sites.

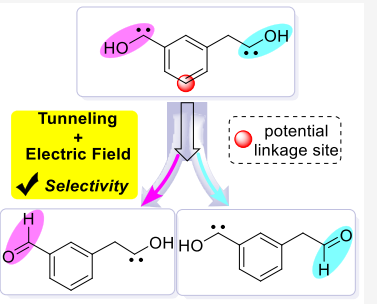

Quantum tunneling (QT), which enables occurrence of reactions and accelerates their rates through barrier penetration, plays an important and unique electronic role in some chemical and enzymatic reactions.[1−13] The probability of quantum tunneling generally increases with decreasing particle mass and/or barrier width (Scheme S1). Consequently, hydrogen tunnels in many reactions.[1−21] Combining experimental and computational methods is a powerful approach that successfully unveils quantum tunneling in many systems and reveals new insights/concepts (e.g., tunneling-controlled reactivity).[22−24]

In addition, some reactions involving rare heavy-atom (mostly carbon) tunneling have been experimentally observed or computationally predicted for various systems, including π-bond-shift, Cope-rearrangement, spin-crossover, biosynthesis, and nucleophilic-substitution (S_N2) reactions, as well as carbon-flipping on a Cu(110) surface and excited-state Zimmerman di-π-methane (DPM) rearrangement (Schemes 1d,e, and S2).[25−40] Our previous computational study predicted the first excited-state heavy-atom tunneling in the DPM rearrangement, which was recently supported by Singleton using his natural abundant ^{13}C NMR experimental method.[41−44] In addition, carbon- and nitrogen-tunneling can compete to form different products via two ring-opening pathways of a benzazirine.[45,46] Moreover, temperature, solvent, isotope or Lewis-acid was also reported to control the tunneling-involving reactions.[47,48] These studies show that several factors ("stimuli") can affect quantum tunneling in some reactions.

The use of an applied external electric field (EEF) is a new electronic approach for controlling the reactivities and selectivities of some chemical and enzymatic reactions.[49−57] Shaik and co-workers reported insightful computational predictions concerning oriented-EEF-controlled reactivity and selectivity in some organic and enzymatic reactions.[56−58] Coote and co-workers reported a seminal experimental and computational study into a classical Diels−Alder reaction accelerated by an EEF (Scheme 1a).[59,60] The Kanan group also demonstrated that an EEF can alter the regioselectivity of a Rh-catalyzed carbene-rearrangement reaction.[61] Encouraged by these successful studies, we hypothesized that reactivity and selectivity can be modulated by combining the two above-mentioned electronic effectors (QT and EEF) and exploiting their synergy.

Inspired by the previous breakthrough,[60] an alkylthiol group as the potential linkage may be added to connect the QT-driven molecules on flat gold surface in the presence of an applied EEF (Scheme 1). However, such studies remain unclear or underdeveloped. In this regard, a recent experiment revealed that the potential energy surface (PES) for the inversion motion of ammonia is altered by a very strong EEF ($\sim 2.0 \times 10^8$ V/m) in a 10 K Ar matrix by using the ice film nanocapacitor method, which leads to the suppression of quantum tunneling.[62] During our investigation, Kozuch and

Received: November 14, 2022
Accepted: January 23, 2023

https://doi.org/10.1021/acs.jpclett.2c03461
J. Phys. Chem. Lett. 2023, 14, 1124−1132

Scheme 1. (a) Schematic Diagram of the EEF-Accelerated Diels–Alder Reaction in Experiments[60] and Our Model Reactions (b–e): (b) Proposed Hypothetic Model of the Hydroxycarbenes Connecting to a Thiolate Linker and Au Cluster/Surface; (c) 1,2-H Migrations of Hydroxycarbenes with Their Measured Half-Lives (τ);[14,16−18] and (d) S_N2 and (e) the Triplet Di-π-methane Rearrangement of Benzobarrelene[a]

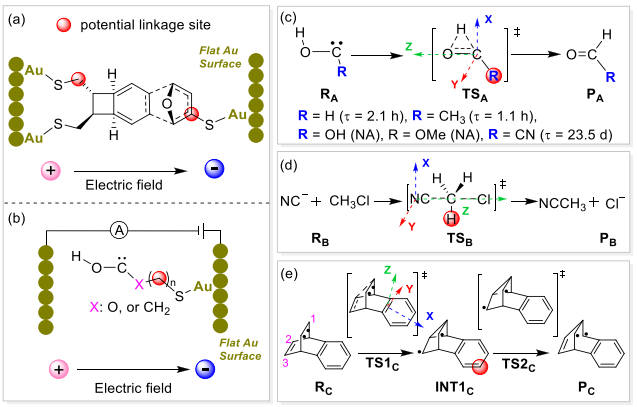

[a]The applied EEF directions are indicated by colored arrows. Red dots denote the potential linkage sites for attaching on the gold surface.

co-workers also reported an independent computational study on the combined QT and EEF on the overall reaction rates of three ground-state carbon-tunneling reactions using a larger EEF (2.6–7.7 V/nm) under cryogenic conditions (Table S1).[63]

In this work, we used reliable density functional theory (DFT) and high-level DLPNO−CCSD(T1) methods in combination with reliable variational transition state theory (VTST) and multidimensional small-curvature tunneling (SCT) correction methods to extensively examine the combined effect of QT and a modest EEF (up to 2.57−5.14 V/nm) on three different reactions (Scheme 1c–e; computational details are given in the Supporting Information).[14,16−18,30,41−43] These three reactions involve hydrogen- or (ground- and excited-state) carbon-tunneling. Our study shows that an oriented EEF can significantly increase or decrease the rate constants for these reactions at low temperatures. In addition, such EEF can also decrease the crossover temperatures ($T_c = \hbar\Omega/(2\pi k_B)$), details in the Supporting Information), transmission coefficient, and quantum tunneling contribution ratio, even though the barrier height and width become smaller. The nontunneling rate constant is generally the key contributor at temperatures above the crossover temperature.[64] Furthermore, our study revealed for the first time that an oriented EEF can control the chemo- or site-selectivity of one single arene molecule with two similar/same reactive sites.

Prior to discussing the effects of QT and an EEF on the computed reaction rate constants and kinetic isotope effects (KIEs) of the above-mentioned three reactions, the most pronounced effect of a Z-EEF on each PES (V_a^G, vibrationally adiabatic ground-state potential energy including minimum energy pathway and zero-point energy) is briefly discussed (Scheme 1 and Figures 1, 3, and 4). Detailed results for the smaller and similar influences of X-EEF or Y-EEF and a weaker Z-EEF are given in Supporting Information. Figures 1, 3, and 4

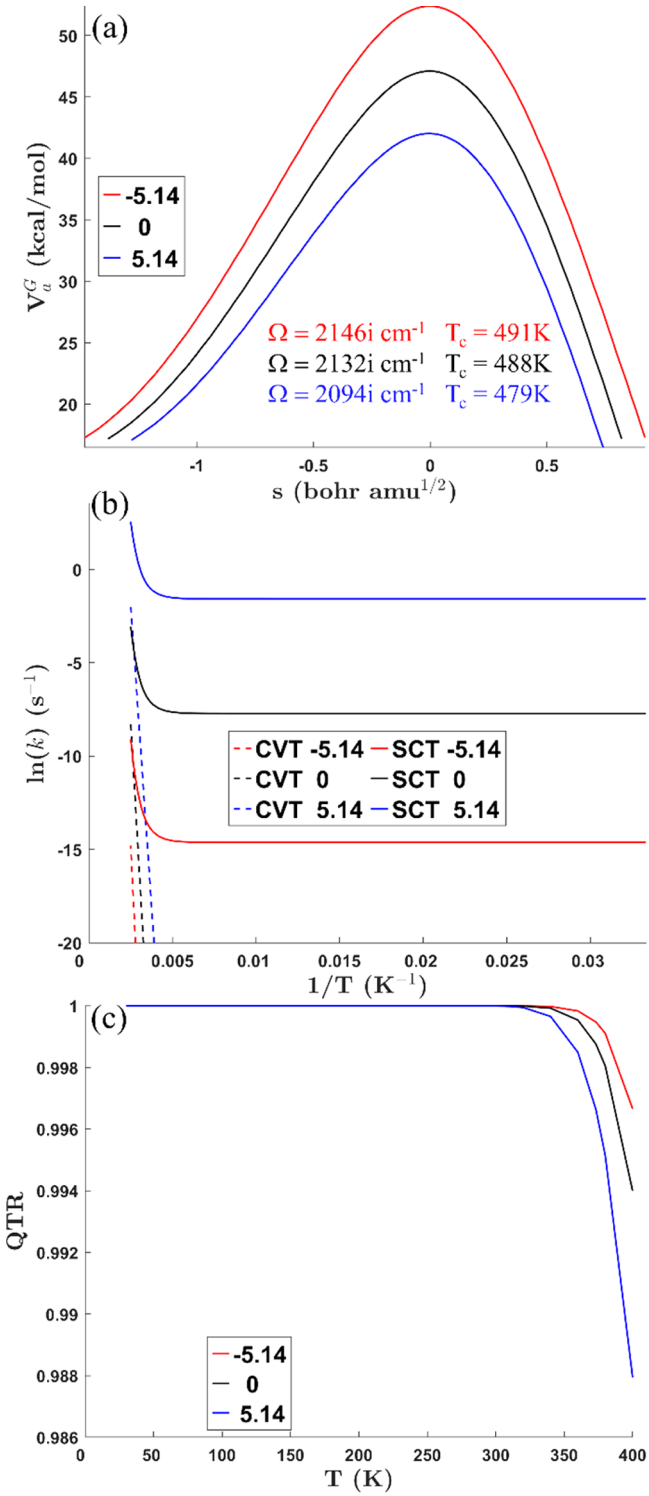

Figure 1. (a) Vibrationally adiabatic ground-state potential energies (V_a^G) for the 1,2-H migration in H−C−OH in a Z-EEF (red, −5.14 V/nm; black, no-EEF (0 V/nm),; blue, 5.14 V/nm) calculated using the ωB97X-D method. (b) Arrhenius plots of computed nontunneling (k_{CVT}, dashed lines) and tunneling-involving (k_{SCT}, solid lines) rate constants. (c) Computed quantum tunneling contribution ratios (QTRs, $k_{SCT}/k_{CVT+SCT}$) as functions of temperature. Ω is the magnitude of the imaginary frequency of the transition state, and T_c is the corresponding crossover temperature.

reveal that a positive Z-EEF reduces both the computed energy barrier and the barrier width (and *vice versa*).[63] Interestingly,

https://doi.org/10.1021/acs.jpclett.2c03461
J. Phys. Chem. Lett. 2023, 14, 1124−1132

Table 1. Computed Rate Constants (k_{CVT} and $k_{CVT+SCT}$ in s^{-1}), Transmission Coefficients (κ_{SCT}), and H/D KIE_{CVT} (Nontunneling) and $KIE_{CVT+SCT}$ (with Tunneling) Values for the 1,2-H Migration in H−C−OH Using the ωB97X-D Method in the Absence or Presence of a Z-EEF (V/nm) at 30, 100, and 200 K

Z-EEF	k_{CVT}	$k_{CVT+SCT}$	κ_{SCT}	KIE_{CVT}	$KIE_{CVT+SCT}$
			30 K		
−5.14	9.10×10^{-247}	4.47×10^{-7}	4.91×10^{239}	8.58×10^{6}	3.49×10^{7}
0	2.47×10^{-208}	4.42×10^{-4}	1.79×10^{204}	7.89×10^{6}	3.78×10^{6}
5.14	9.85×10^{-172}	2.04×10^{-1}	2.08×10^{170}	6.52×10^{6}	3.05×10^{5}
			100 K		
−5.14	8.91×10^{-66}	4.47×10^{-7}	5.02×10^{58}	1.21×10^{2}	3.49×10^{7}
0	2.99×10^{-54}	4.42×10^{-4}	1.48×10^{50}	1.18×10^{2}	3.78×10^{6}
5.14	2.84×10^{-43}	2.05×10^{-1}	7.19×10^{41}	1.11×10^{2}	3.07×10^{5}
			200 K		
−5.14	8.40×10^{-27}	4.87×10^{-7}	5.80×10^{19}	1.10×10^{1}	1.72×10^{7}
0	4.83×10^{-21}	4.77×10^{-4}	9.87×10^{16}	1.09×10^{1}	1.94×10^{6}
5.14	1.48×10^{-15}	2.19×10^{-1}	1.48×10^{14}	1.06×10^{1}	1.83×10^{5}

the lower and thinner barriers were found to have lower crossover temperatures (T_c). The large reduction in the barrier is attributable to larger favorable electrostatic stabilization in the transition state relative to the reactant in the presence of the Z-EEF (Figures S1−S9), as the charged moieties move parallel to the Z-EEF direction in the first two systems. Moreover, both k_{CVT} and $k_{CVT+SCT}$ are generally linear and temperature-dependent in the absence or presence of the EEF at high temperatures, whereas $k_{CVT+SCT}$ becomes nonlinear or even temperature-independent at (very) low temperatures (i.e., the deep-tunneling region).

Effect of EEF on H-Tunneling in Hydroxycarbenes. Figure 1 summarizes the PESs (V_a^G) as well as the nontunneling and tunneling-involving rate constants (k_{CVT} and k_{SCT}) for the 1,2-H migration in H−C−OH in the absence (0 V/nm, "no-EEF") and presence of a ±5.14 V/nm Z-EEF. As the positive Z-EEF direction is roughly parallel to the direction of the electron-deficient hydrogen (proton) migration, more electrostatic stabilization gained in the transition states (relative to the reactants) leads to lower the energy barrier by about 5.1 kcal/mol compared to the no-EEF case (Figure 1a). However, the barrier is increased by ∼5.3 kcal/mol when the negative Z-EEF (in opposite to the proton migration direction) is applied. Therefore, on the basis of (variational) transition-state theory, the nontunneling rate constant (k_{CVT}) is considerably enhanced by ∼36 orders of magnitude in the positive Z-EEF at 30 K (and *vice versa*, Table 1). However, this enhancement decreases significantly with increasing temperature. Notably, the magnitude of the nontunneling rate constant at 30 K is extremely small ($<10^{-172}$ s^{-1}), irrespective of the absence or presence of the EEF.

Compared to the negligible k_{CVT} values, the significant and temperature-independent (up to ∼200 K) tunneling-involving rate constants ($k_{SCT} \approx k_{CVT+SCT}$, $\sim 10^{-7}$−10^{-1} s^{-1}) in the absence or presence of the EEF support the notion that this 1,2-H migration is heavily controlled by hydrogen tunneling (Figure 1b,c), which is reflected in their tremendous transmission coefficients (κ_{SCT}).[16] In addition, the quantum tunneling contributions (ratio) to the overall rate constants (QTR = $k_{SCT}/k_{CVT+SCT}$) are very high even at high temperatures (>99.8% at ∼350 K), and they also increase with increasing crossover temperature (T_c = 479−491 K, Figure 1a, c). Moreover, both $k_{CVT+SCT}$ and k_{SCT} are significantly larger in magnitude in the positive Z-EEF through hydrogen tunneling than those in the absence of the EFF. Nevertheless, the positive Z-EEF slightly lowers crossover temperature and the quantum tunneling contribution ratio (QTR) surprisingly.

Comparatively, these rate constants ($k_{CVT+SCT}$ and k_{SCT}) are diminished in the negative Z-EEF along with slightly higher T_c and QTR values. For instance, compared with $k_{CVT+SCT}$ in the absence of an EEF at 30 K (4.42×10^{-4} s^{-1}), $k_{CVT+SCT}$ is about three-orders-of-magnitude higher in the positive Z-EEF ($k_{CVT+SCT} = 2.04 \times 10^{-1}$ s^{-1}) and correspondingly lower in the negative Z-EEF ($k_{CVT+SCT} = 4.47 \times 10^{-7}$ s^{-1}). This three-orders-of-magnitude enhancement/reduction in $k_{CVT+SCT}$ by the positive/negative Z-EEF is roughly maintained in the 30−200 K range, where each dominant k_{SCT} component is approximately independent of temperature (deep-tunneling region). Overall, compared to the no-EEF case, the lower and thinner barrier induced by the positive Z-EEF enhances all rate constants (i.e., k_{CVT}, k_{SCT}, and $k_{CVT+SCT}$), while the corresponding crossover temperature, transmission coefficients and quantum tunneling contribution ratio are slightly diminished surprisingly. Similar features and trends were also observed for the other four examined hydroxycarbenes (R-C−OH; R = CH_3, OH, OCH_3, and CN; see Supporting Information).

Moreover, the H/D KIE_{CVT} determined in the absence of tunneling for H-migration in H−C−OH/D was found to be hardly affected by the Z-EEF (Table 1). However, hydrogen tunneling generally led to a significantly higher H/D $KIE_{CVT+SCT}$ relative to the H/D KIE_{CVT} at low temperatures (30−200 K), except in the absence of the EEF or when the positive Z-EEF is applied at very low temperatures (Figure S16c). The enhanced H/D $KIE_{CVT+SCT}$ values associated with quantum tunneling are qualitatively consistent with the correspondingly large transmission coefficients (κ_{SCT}). Moreover, the H/D $KIE_{CVT+SCT}$ values at 30−200 K in the positive Z-EEF are smaller than those observed in the absence of the EEF (and *vice versa*), which is consistent with smaller QTR and κ_{SCT} values in the positive Z-EEF. These results show that hydrogen tunneling and a Z-EEF can significantly affect the H/D $KIE_{CVT+SCT}$ value at low temperatures (below 200 K).

Interestingly, the Schreiner group reported that some "reactive" systems (e.g., R = H or CH_3) can quickly undergo H-migration, while migration hardly proceeds for some less-reactive hydroxycarbenes (e.g., R = CN, OH, or OCH_3) under cryogenic conditions.[14−19] We further investigated the ability of a Z-EEF to modulate the reactivities/half-lives of these five

https://doi.org/10.1021/acs.jpclett.2c03461
J. Phys. Chem. Lett. 2023, 14, 1124−1132

hydroxycarbenes. The computed half-lives (τ) at 30 K in the absence of an EEF are comparable to the measured results (Table 2).[14−19] H−C−OH and H_3C−C−OH have the computed τ values of ∼ 0.4−2.9 h, while the computed half-lives for HO−C−OH, MeO−C−OH and NC−C−OH are 285, 1976, and 18 days, respectively.

Table 2. Half-Lives for Hydrogen Tunneling in Five Hydroxycarbenes (R−C−OH; R = H, CH_3, OH, OCH_3, CN) in a Z-EEF (V/nm) at 30 K Computed Using the ωB97X-D Method[a]

	R = H	R = CH_3	R = OH	R = OCH_3	R = CN
−5.14	17.9 d	176.7 d	1592.4 y	19450.9 y	16.2 y
0	0.4 h	2.9 h	285.4 d	1976.0 d	17.6 d
EXP	2.1 h	1.1 h	NA[b]	NA[b]	23.5 d
5.14	0.1 min	0.2 min	6.4 h	32.1 h	2.3 h

[a]Measured half-lives (EXP) for these hydroxycarbenes in the absence of an EEF (0 V/nm) are taken from refs 14 and 16−18. [b]No reaction observed.

In the negative Z-EEF (−5.14 V/nm), the computed half-life for the "reactive" H−C−OH or H_3C−C−OH is considerably elongated from 0.4−2.9 h (no-EEF) to ∼18−177 days (Z-EEF). Consequently, the "reactive" H−C−OH or H_3C−C−OH is expected to experimentally exhibit negligible H-migration in the negative Z-EEF (2 h). On the other hand, the positive Z-EEF (5.14 V/nm) substantially shortens the computed half-lives of these hydroxycarbenes (R = H or CH_3, 0.1−0.2 min; R = CN, 2.3 h; R = OH, 6.4 h; R = OCH_3, 32.1 h). Notably, the hydrogen migration of "inactive" HO−C−OH or CH_3O−C−OH was not observed experimentally (cf.: the computed half-life is ∼285−1976 days) due to stabilization of the carbene carbon by the π-donating oxygen atom.[18] However, H-migration of the least-reactive HO−C−OH, NC−C−OH, or CH_3O−C−OH could become feasible in the positive Z-EEF (5.14 V/nm), with a computed half-life of 2.3−32.1 h only. Hence, the hydrogen migration of some "inactive" hydroxycarbenes in a positive Z-EEF may be experimentally observed in (slightly) longer reaction time (hours-to-days) or in shorter time using a stronger EEF. Overall, our computational predictions show that including a suitable EEF in the hydrogen-migration direction can turn on ("stimulate") or turn off ("inhibit") H-migration in hydroxycarbenes.

Predicting EEF-Controlled Chemo- or Site-Selectivity. Encouraged by the above-mentioned predictions for the EEF-controlled reactivities associated with hydrogen migration (Tables 1 and 2), we further explored the feasibility of a Z-EEF to control chemo- or site-selectivity during hydrogen migration in two arene derivatives ($\mathbf{R_D}$ and $\mathbf{R_E}$), each bearing two hydroxycarbene moieties with the same or similar reactivities (Figure 2 and Table 3).

Figure 2c and Table 3 show that the $k_{(CVT+SCT)A}/k_{(CVT+SCT)B}$ (selectivity factor) computed for the chemoselective H-migration of $\mathbf{R_D}$ increased from 2.9 (no-EEF) to 116.6 when the positive Z_A-EEF was applied under cryogenic conditions. Pleasingly, these results suggest that the migration reaction on the benzyl-substituted carbene proceeds faster (with the selectivity factor of 116.6) along path A to give $\mathbf{PA_D}$ as the major product over path B in the positive Z_A-EEF at 30 K. In

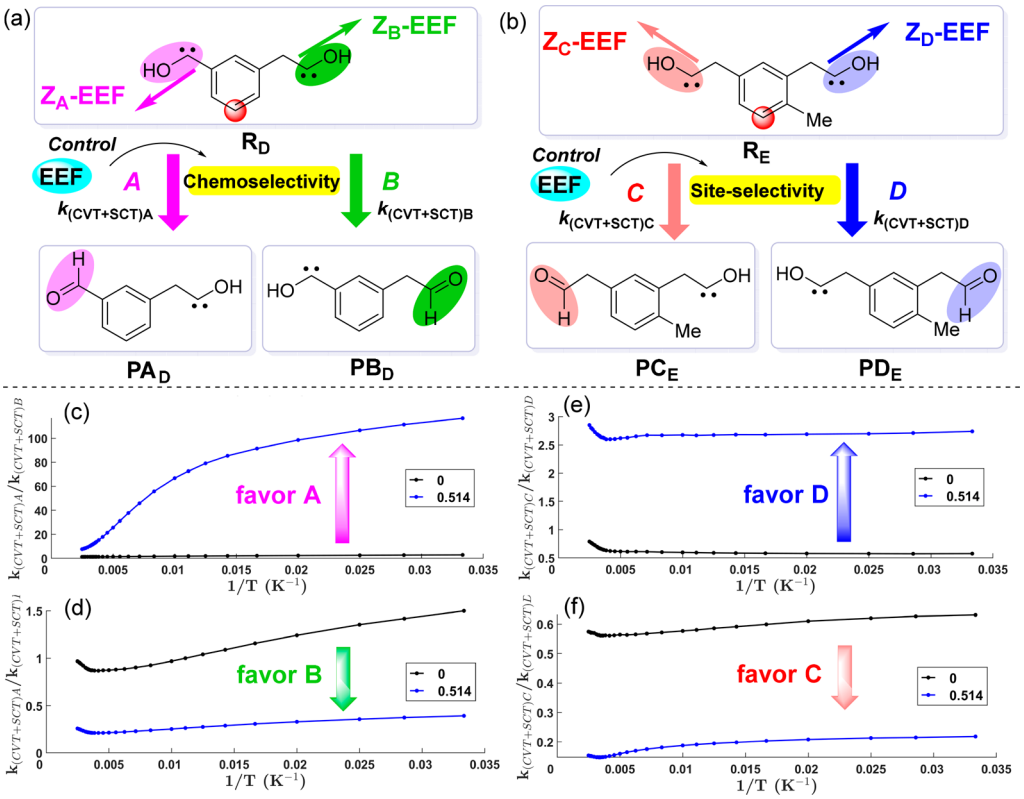

Figure 2. Schematic depicting chemoselectivity during H-migration in (a) $\mathbf{R_D}$ and (b) $\mathbf{R_E}$ bearing two different hydroxycarbene moieties in EEFs. Plots of $k_{(CVT+SCT)A}/k_{(CVT+SCT)B}$ vs 1/T for $\mathbf{R_D}$ or $\mathbf{R_E}$ calculated using the ωB97X-D method in (c) Z_A-EEF, (d) Z_B-EEF, (e) Z_C-EEF, and (f) Z_D-EEF (black, no-EEF (0 V/nm), and blue, 0.514 V/nm). The red dot denotes the potential linkage site for attaching on the gold surface.

https://doi.org/10.1021/acs.jpclett.2c03461
J. Phys. Chem. Lett. 2023, 14, 1124−1132

Table 3. Rate Constants (in s^{-1}), Selectivity Factor (Ratio of the Rate Constants, k_A/k_B), Half-Life (τ, h), and its Half-Life Difference ($\Delta\tau$, h) at 30 K for the Chemo- or Site-Selectivities of R_D and R_E in the Z_A-, Z_B-, Z_C-, and Z_D-EEFs with Various EEF Strengths Calculated Using the ωB97X-D Method

	$k_{(CVT+SCT)A}$	$k_{(CVT+SCT)B}$	k_A/k_B[a]	τ_A	τ_B	$\Delta\tau_{(A-B)}$
			R_D (chemoselectivity): Z_A-EEF direction			
−0.514	1.53×10^{-5}	3.01×10^{-5}	0.5	12.6	6.4	6.2
0	3.72×10^{-5}	1.30×10^{-5}	2.9	5.2	14.8	−9.6
0.514	7.22×10^{-5}	6.19×10^{-7}	116.6	2.7	311.0	−308.3
			R_D (chemoselectivity): Z_B-EEF direction			
−0.514	3.69×10^{-5}	4.96×10^{-6}	7.4	5.2	38.8	−33.6
0	1.77×10^{-5}	1.18×10^{-5}	1.5	10.9	16.3	−5.4
0.514	1.28×10^{-5}	3.25×10^{-5}	0.4	15.0	5.9	9.1
	$k_{(CVT+SCT)C}$	$k_{(CVT+SCT)D}$	k_C/k_D[a]	τ_C	τ_D	$\Delta\tau_{(C-D)}$
			R_E (site-selectivity): Z_C-EEF direction			
−0.514	7.40×10^{-6}	5.84×10^{-5}	0.1	26.0	3.3	22.7
0	2.04×10^{-5}	3.54×10^{-5}	0.6	9.4	5.4	4.0
0.514	4.08×10^{-5}	1.49×10^{-5}	2.7	4.7	12.9	−8.2
			R_E (site-selectivity): Z_D-EEF direction			
−0.514	3.51×10^{-5}	1.34×10^{-5}	2.6	5.5	14.4	−8.9
0	1.85×10^{-5}	2.93×10^{-5}	0.6	10.4	6.6	3.8
0.514	9.52×10^{-6}	4.36×10^{-5}	0.2	20.2	4.4	15.8

[a]The k_A/k_B means $k_{(CVT+SCT)A}/k_{(CVT+SCT)B}$; the k_C/k_D means $k_{(CVT+SCT)C}/k_{(CVT+SCT)D}$

addition, the corresponding absolute half-life difference is calculated to be ~308.3 h. On the other hand, the chemoselectivity of the H-migration of $\mathbf{R_D}$ can be reversed (via path B) to form $\mathbf{PB_D}$ as the major product by applying a positive Z_B-EEF under cryogenic conditions (Figure 2d and Table 3).

Similar EEF-controlled site-selectivities were observed for the H-migration of $\mathbf{R_E}$ bearing the same carbene groups by including a Z_C-EEF or Z_D-EEF (Figure 2, parts e and f). Namely, the selectivity factor ($k_{(CVT+SCT)C}/k_{(CVT+SCT)D}$) for the H-migration in $\mathbf{R_E}$ decreases from 0.6 (no-EEF) to 0.2 (positive Z_D-EEF) under cryogenic conditions. These results suggest that the reaction proceeds faster along path D to afford $\mathbf{PD_E}$ as the major product than path C under positive Z_D-EEF conditions. Also, the computed corresponding half-life differences is ~15.8 h at 30 K. On the other hand, $\mathbf{R_E}$ can undergo the opposite site-selective H-migration to form $\mathbf{PC_E}$ as the major product (via path C) in the positive Z_C-EEF under cryogenic conditions (Figure 2e, 2f).[65] Similarly, the results of different EEF directions are summarized in Table 3. To the best of our knowledge, our study suggests for the first time that an EEF can modulate the chemo- or site-selectivity of reactions that involve tunneling.

Effect of EEF on Tunneling in the S_N2 Reaction. The classical S_N2 reaction shown in Scheme 1d was recently predicted to involve considerable quantum tunneling by Greer and Doubleday.[30] As depicted in Figure 3a, our computational results suggest that, compared to the no-EEF case, a modest Z-EEF (±1.54 V/nm) significantly affects the PES for the S_N2 reaction. The energy barrier can be decreased by ~4.5 kcal/mol in the positive Z-EEF and increased by ~5.1 kcal/mol in the negative Z-EEF. The CN anion attacks CH_3Cl accompanied by dissociation of the Cl anion on the opposite side in this S_N2 reaction, in which direction of the formal negative charge relocation is parallel to the positive Z-EEF direction (Figures S3 and S8). Accordingly, the larger barrier reduction in the positive Z-EEF results from greater electrostatic stabilization in the transition state (with respect to the reactant). A large polarization in the transition states in the Z-EEF reinforces this electrostatic stabilization. Apart from the lower energy barrier, the positive Z-EEF also narrows the barrier (and *vice versa*), albeit with a slightly smaller crossover temperature.

Moreover, carbon tunneling makes a dominant contribution to the overall rate constant ($k_{CVT+SCT}$) below T_c (131−145 K), whereas the nontunneling (overbarrier) rate constant (k_{CVT}) is the key contributor at high temperatures (>200 K, Figure 3b and Table 4). For example, compared to the no-EEF case at 100 K, $k_{CVT+SCT}$ is enhanced by about seven-orders-of-magnitude in the positive Z-EEF. On the contrary, $k_{CVT+SCT}$ is seven-orders-of-magnitude lower in the negative Z-EEF compared to that determined in the absence of an EEF. Similarly, $k_{CVT+SCT}$ was enhanced/reduced by around three- or four-orders-of-magnitude in the positive/negative Z-EEF at 300 K, compared to the no-EEF case. It should be noted that the transmission coefficient (κ_{SCT}) was enhanced by three-orders-of-magnitude in the negative Z-EEF (and *vice versa*) at 100 K (below T_c), but was only marginally affected by the Z-EEF above T_c (>200 K). Therefore, the enhancement in the overall rate constant ($k_{CVT+SCT}$) observed at high temperatures is mainly ascribable to the increase in the nontunneling (overbarrier) rate constant (k_{CVT}) due to its lower energy barrier induced by the Z-EEF.

Moreover, $^{12}C/^{13}C$ KIE_{CVT} values computed without tunneling are quite similar in the absence or presence of the Z-EEF: 1.10−1.16 (100 K), 1.03−1.08 (200 K), and 1.01−1.06 (300 K), as summarized in Table 4. On the contrary, the $^{12}C/^{13}C$ $KIE_{CVT+SCT}$ (8.90 in −1.54 V/nm and 2.87 in 1.54 V/nm at 100 K) values computed with tunneling are strongly affected by the Z-EEF at low temperatures, compared with the non-EEF case ($KIE_{CVT+SCT}$: 4.33). However, the $^{12}C/^{13}C$ $KIE_{CVT+SCT}$ values were found to be only slightly affected by Z-EEF at higher temperatures (200−300 K) due to their similar κ_{SCT} values. These results demonstrate that an EEF also affects the reactivity and $^{12}C/^{13}C$ KIE of this heavy-atom-tunneling reaction, albeit to a smaller extent than the H-migration case.

Effect of EEF on Tunneling in the Triplet DPM Rearrangement Reaction. Since the effect of an EEF on an excited-state reaction

https://doi.org/10.1021/acs.jpclett.2c03461
J. Phys. Chem. Lett. 2023, 14, 1124−1132

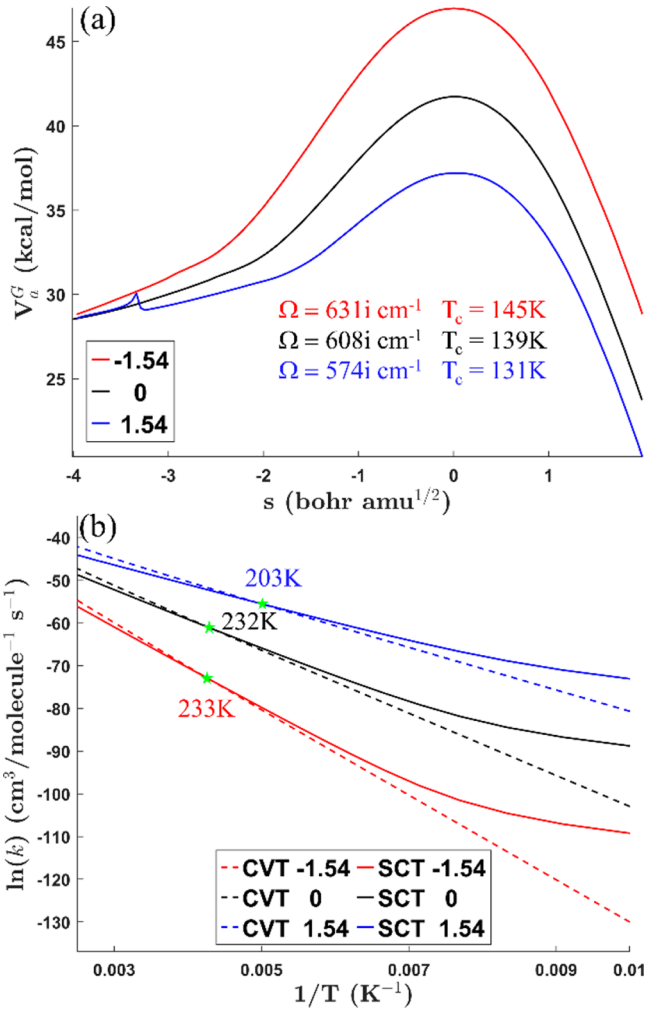

Figure 3. (a) Vibrationally adiabatic ground-state potential energies (V_a^G) for the S_N2 reaction calculated using the M06-2X method. (b) Arrhenius plots of the nontunneling (k_{CVT}, dashed lines) and tunneling-involving (k_{SCT}, solid lines) rate constants in the Z-EEF (red, −1.54 V/nm; black, no EEF (0 V/nm); and blue, 1.54 V/nm). Ω is the magnitude of the imaginary frequency for the transition state, and T_c is the corresponding crossover temperature.

that involves tunneling has not been examined previously, we investigated how EEF affects the first C−C-forming step of the triplet DPM rearrangement reaction (the first excited-state heavy-atom tunneling reaction).[41] While the DPM rearrangement of benzobarrelene exhibited a 1.6 kcal/mol lower barrier height and thinner barrier width in a negative Z-EEF of −5.14 V/nm compared to the no-EEF case, only a slightly lower T_c was observed (Figure 4 and Table 5). Similar to the S_N2 reaction, excited-state carbon tunneling makes a dominant contribution to the overall rate constant ($k_{CVT+SCT}$) below T_c (126−140 K), in which the tunneling-involving rate constant is vital. On the other hand, excited-state carbon tunneling becomes less important at higher temperatures (i.e., 200−300 K above T_c), where κ_{SCT} becomes much smaller. Notably, carbon tunneling cannot be overlooked at high temperatures (200−300 K), as a QTR (C-tunneling contribution ratio) of about 20−50% was observed.

Also, the value of $k_{CVT+SCT}$ in the negative Z-EEF is about two-orders-of-magnitude higher than that observed in the absence of an EEF at 100 K. However, the roughly one-order-of-magnitude enhanced $k_{CVT+SCT}$ resulting from this negative Z-EEF is almost maintained at higher temperatures (200−300 K, Table 5). Taken together, the EEF-enhanced overall rate constant for the triplet DPM rearrangement at 200 K is attributable to both higher nontunneling (overbarrier) and tunneling-involving (through-barrier) rate constants. The latter one is found to contribute less to the overall rate constant with increasing temperature. In addition, as was observed for the H-migration and S_N2 reactions, the lower and thinner barriers induced by the EEF also feature smaller T_c, κ_{SCT} and QTR.

^{13}C was substituted for ^{12}C at the C1, C2, and C3 positions of benzobarrelene to further evaluate $^{12}C/^{13}C$ KIE_{CVT} (without tunneling) and $KIE_{CVT+SCT}$ (with tunneling) values for the DPM rearrangement. Although the $^{12}C/^{13}C$ KIE_{CVT} value was the same in the presence and absence of the Z-EEF at 100 K (i.e., 1.18), $^{12}C/^{13}C$ $KIE_{CVT+SCT}$ was calculated to be smaller in the Z-EEF at 100 K than that in the non-EEF case (1.36 vs 1.54). Nevertheless, the Z-EEF hardly changes the $^{12}C/^{13}C$ $KIE_{CVT+SCT}$ value at high temperatures (200−300 K). Taken together, our study suggests that an EEF can also influence the reactivity and $^{12}C/^{13}C$ KIE of this excited-state heavy-atom tunneling reaction, but to a lesser extent than the H-migration case.

In summary, our extensive computational study revealed that an appropriately orientated EEF can (significantly) affect the overall rate constants and KIEs associated with three different

Table 4. Rate Constants (k_{CVT} and $k_{CVT+SCT}$, L mol^{-1} s^{-1}), Transmission Coefficients (κ_{SCT}), and $^{12}C/^{13}C$ KIE_{CVT} and $KIE_{CVT+SCT}$ Values without and with Tunneling, Respectively, for the S_N2 Reaction in a Z-EEF (V/nm) Calculated Using the M06-2X Method at 100, 200, and 300 K

Z-EEF	k_{CVT}	$k_{CVT+SCT}$	κ_{SCT}	KIE_{CVT}	$KIE_{CVT+SCT}$
		100 K			
−1.54	2.03×10^{-36}	2.19×10^{-27}	1.07×10^{9}	1.11	8.90
0	1.16×10^{-24}	1.67×10^{-18}	1.44×10^{6}	1.16	4.33
1.54	5.60×10^{-15}	1.13×10^{-11}	2.01×10^{3}	1.10	2.87
		200 K			
−1.54	7.89×10^{-15}	2.17×10^{-14}	2.75	1.04	1.16
0	8.97×10^{-9}	2.44×10^{-8}	2.72	1.08	1.17
1.54	4.71×10^{-4}	9.51×10^{-4}	2.02	1.03	1.10
		300 K			
−1.54	1.82×10^{-7}	2.68×10^{-7}	1.48	1.01	1.05
0	2.66×10^{-3}	3.93×10^{-3}	1.47	1.06	1.08
1.54	3.05	3.96	1.30	1.01	1.04

https://doi.org/10.1021/acs.jpclett.2c03461
J. Phys. Chem. Lett. 2023, 14, 1124−1132

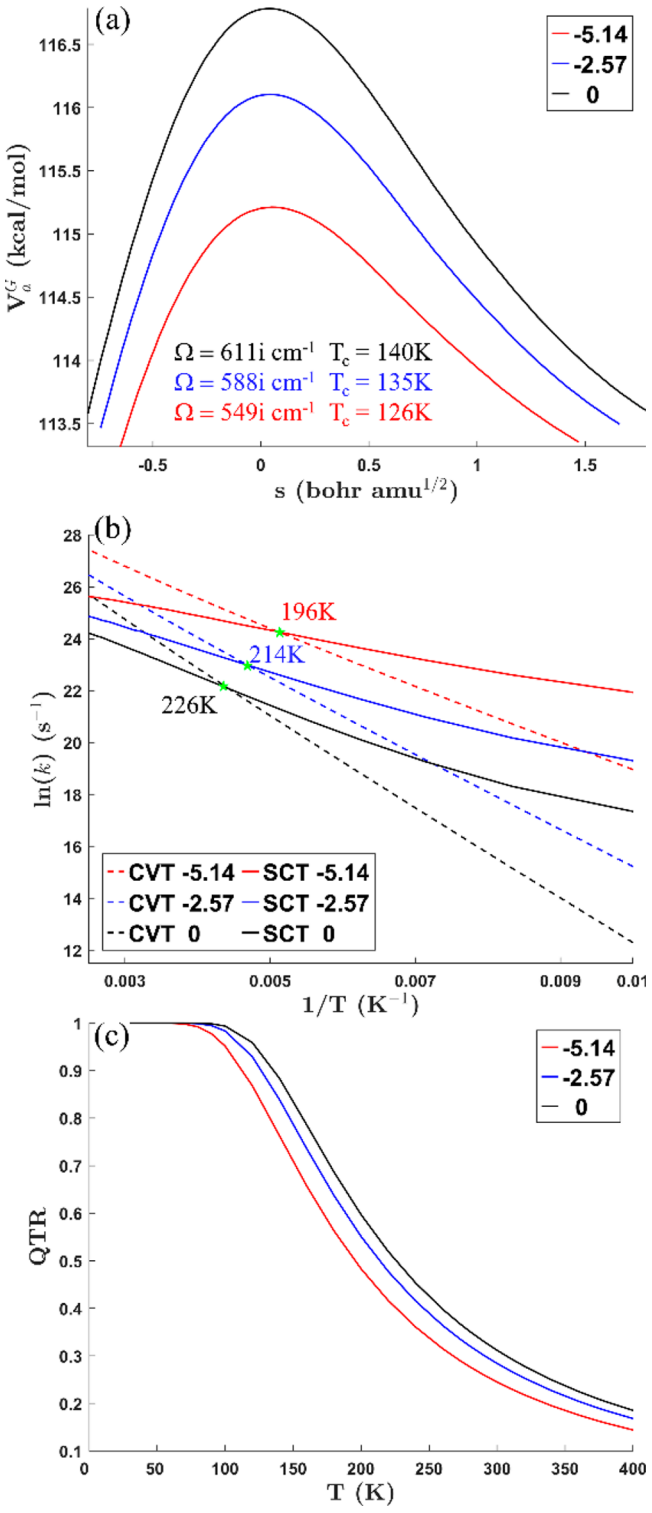

Figure 4. (a) Vibrationally adiabatic ground-state potential energies (V_a^G) for the triplet DPM rearrangement of benzobarrelene calculated by the ωB97X-D method. (b) Arrhenius plots of the nontunneling (k_{CVT}, dashed lines) and tunneling-involving (k_{SCT}, solid lines) rate constants in the Z-EEF (red, −5.14 V/nm; black, no EEF (0 V/nm); and blue, −2.57 V/nm). (c) Quantum tunneling contribution ratios (QTR, $k_{SCT}/k_{CVT+SCT}$) as functions of temperatures. Ω is the magnitude of the imaginary frequency for the transition state, and T_c is the corresponding crossover temperature.

reactions involving hydrogen and (ground- and excited-state) carbon tunneling (i.e., the 1,2-H migrations of hydroxycarbenes, S_N2 and triplet Zimmerman DPM rearrangement reactions). *An oriented EEF applied in a manner that decreases both the energy barrier and barrier width (especially along the reaction axis) enhances the magnitude of the overall rate constant* as well as both nontunneling (overbarrier) and tunneling-involving (through-barrier) rate constants. The lower energy barriers are ascribed to more electrostatic stabilization in the transition states than the reactants under EEF. Unexpectedly, these EEF effects also *slightly decrease the crossover temperature, transmission coefficient and quantum tunneling contribution ratio*, even though the barrier width is narrower and barrier height is reduced. Quantum tunneling was found to contribute the most to the overall reaction rate constant at temperatures below T_c, while, the nontunneling rate constant contributes more with increasing temperature. In addition, H-migration reactivity in hydroxycarbenes can be varied or even "switched on/off" by the EEF. In particular, the 1,2-H migration of "inactive" HO-C−OH, CH_3O−C−OH, or NC-C−OH is predicted to be possibly experimentally observable in a modest (~5.14 V/nm) or stronger EEF. Moreover, our study demonstrated for the first time that the chemo- or site-selectivity of one single arene molecule with the two same or similar reactive sites can be controlled and switched by applying an EEF. Given that an EEF-accelerated Diels−Alder reaction was successfully realized,[60] our computational results suggest that an EEF can act as a potentially useful electronic effector (external stimulus) capable of on/off-switching or modulating the reactivities and selectivities of some tunneling-involving reactions in chemical and enzymatic systems around charged and/or confined reaction environments.[50,57,66]

Table 5. Rate Constants (k_{CVT} and $k_{CVT+SCT}$, in s^{-1}), Transmission Coefficients (κ_{SCT}), and $^{12}C/^{13}C$ KIE_{CVT} and $KIE_{CVT+SCT}$ Values without and with Tunneling, Respectively, for the First Step in the DPM Rearrangement of Benzobarrelene Computed Using the ωB97X-D Method in a −5.14 V/nm Z-EEF and in the Absence of an EEF (0 V/nm) at 100, 200, and 300 K

Z-EEF	k_{CVT}	$k_{CVT+SCT}$	κ_{SCT}	KIE_{CVT}	$KIE_{CVT+SCT}$
		100 K			
−5.14	1.71×10^{8}	3.53×10^{9}	20.64	1.18	1.36
0	2.18×10^{5}	3.43×10^{7}	157.34	1.18	1.54
		200 K			
−5.14	3.94×10^{10}	7.63×10^{10}	1.94	1.09	1.15
0	1.37×10^{9}	3.41×10^{9}	2.49	1.09	1.16
		300 K			
−5.14	2.85×10^{11}	3.78×10^{11}	1.33	1.06	1.09
0	2.97×10^{10}	4.32×10^{10}	1.45	1.07	1.09

■ ASSOCIATED CONTENT

Supporting Information

The Supporting Information is available free of charge at https://pubs.acs.org/doi/10.1021/acs.jpclett.2c03461.

Detailed computational and results, Cartesian coordinates, and energies of all optimized structures (PDF)
Transparent Peer Review report available (PDF)

■ AUTHOR INFORMATION

Corresponding Authors

Lung Wa Chung − *Shenzhen Grubbs Institute, Department of Chemistry, and Guangdong Provincial Key Laboratory of*

https://doi.org/10.1021/acs.jpclett.2c03461
J. Phys. Chem. Lett. 2023, 14, 1124−1132

Catalysis, Southern University of Science and Technology, Shenzhen 518055, P. R. China; orcid.org/0000-0001-9460-7812; Email: oscarchung@sustech.edu.cn

Xin Li − *Shenzhen Grubbs Institute, Department of Chemistry, and Guangdong Provincial Key Laboratory of Catalysis, Southern University of Science and Technology, Shenzhen 518055, P. R. China;* orcid.org/0000-0003-4026-9365; Email: lix7@sustech.edu.cn

Authors

Zhifeng Ma − *Shenzhen Grubbs Institute, Department of Chemistry, and Guangdong Provincial Key Laboratory of Catalysis, Southern University of Science and Technology, Shenzhen 518055, P. R. China*

Zeyin Yan − *Shenzhen Grubbs Institute, Department of Chemistry, and Guangdong Provincial Key Laboratory of Catalysis, Southern University of Science and Technology, Shenzhen 518055, P. R. China*

Complete contact information is available at: https://pubs.acs.org/10.1021/acs.jpclett.2c03461

Author Contributions

‡Z.M. and Z.Y. contributed equally to this work.

Notes

The authors declare no competing financial interest.

■ ACKNOWLEDGMENTS

This work is dedicated to Professor Xueming Yang on the occasion of his 60th birthday. We thank Prof. Donald G. Truhlar and Dr. Jingjing Zheng for helpful advice on Polyrate calculations with an EEF. Financial support by the National Natural Science Foundation of China (21873043, 21933003, 22193020, and 22193023), SUSTech, the Shenzhen Nobel Prize Scientists Laboratory Project (C17783101), and the Guangdong Provincial Key Laboratory of Catalysis (2020B121201002) are acknowledged. We also thank the Center for Computational Science and Engineering and the CHEM high performance supercomputer cluster (CHEM-HPC) at SUSTech for partly supporting this work

■ REFERENCES

(1) Nagel, Z. D.; Klinman, J. P. Tunneling and dynamics in enzymatic hydride transfer. *Chem. Rev.* **2006**, *106*, 3095−3118.
(2) Truhlar, D. G. Tunneling in enzymatic and nonenzymatic hydrogen transfer reactions. *J. Phys. Org. Chem.* **2010**, *23*, 660−676.
(3) Ley, D.; Gerbig, D.; Schreiner, P. R. Tunnelling control of chemical reactions−the organic chemist's perspective. *Org. Biomol. Chem.* **2012**, *10*, 3781−3790.
(4) Kästner, J.; Kozuch, S. *Tunnelling in Molecules*; Royal Society of Chemistry: 2020.
(5) Castro, C.; Karney, W. L. Heavy-Atom Tunneling in Organic Reactions. *Angew. Chem., Int. Ed.* **2020**, *59*, 8355−8366.
(6) Karmakar, S.; Datta, A. Heavy-atom tunneling in organic transformations. *J. Chem. Sci.* **2020**, *132*, 1−22.
(7) Borden, W. T. Reactions that involve tunneling by carbon and the role that calculations have played in their study. *Wiley Interdiscip. Rev.: Comput. Mol. Sci.* **2016**, *6*, 20−46.
(8) Schreiner, P. R. Quantum Mechanical Tunneling Is Essential to Understanding Chemical Reactivity. *Trends Chem.* **2020**, *2*, 980−989.
(9) Schreiner, P. R. Tunneling Control of Chemical Reactions: The Third Reactivity Paradigm. *J. Am. Chem. Soc.* **2017**, *139*, 15276−15283.
(10) Greer, E. M.; Kwon, K.; Greer, A.; Doubleday, C. Thermally activated tunneling in organic reactions. *Tetrahedron* **2016**, *72*, 7357−7373.
(11) Meisner, J.; Kastner, J. Atom Tunneling in Chemistry. *Angew. Chem., Int. Ed.* **2016**, *55*, 5400−5413.
(12) Dale, H. J. A.; Leach, A. G.; Lloyd-Jones, G. C. Heavy-Atom Kinetic Isotope Effects: Primary Interest or Zero Point? *J. Am. Chem. Soc.* **2021**, *143*, 21079−21099.
(13) Pu, J. Z.; Gao, J. L.; Truhlar, D. G. Multidimensional tunneling, recrossing, and the transmission coefficient for enzymatic reactions. *Chem. Rev.* **2006**, *106*, 3140−3169.
(14) Eckhardt, A. K.; Erb, F. R.; Schreiner, P. R. Conformer-specific [1,2]H-tunnelling in captodatively-stabilized cyanohydroxycarbene (NC−C−OH). *Chem. Sci.* **2019**, *10*, 802−808.
(15) Mardyukov, A.; Quanz, H.; Schreiner, P. R. Conformer-specific hydrogen atom tunnelling in trifluoromethylhydroxycarbene. *Nat. Chem.* **2017**, *9*, 71−76.
(16) Schreiner, P. R.; Reisenauer, H. P.; Pickard, F. C.; Simmonett, A. C.; Allen, W. D.; Matyus, E.; Csaszar, A. G. Capture of hydroxymethylene and its fast disappearance through tunnelling. *Nature* **2008**, *453*, 906−909.
(17) Schreiner, P. R.; Reisenauer, H. P.; Ley, D.; Gerbig, D.; Wu, C. H.; Allen, W. D. Methylhydroxycarbene: Tunneling Control of a Chemical Reaction. *Science* **2011**, *332*, 1300−1303.
(18) Schreiner, P. R.; Reisenauer, H. P. Spectroscopic identification of dihydroxycarbene. *Angew. Chem., Int. Ed.* **2008**, *47*, 7071−7074.
(19) Kästner, J. Path Length Determines the Tunneling Decay of Substituted Carbenes. *Chem. Eur. J.* **2013**, *19*, 8207−8212.
(20) Xie, C.; Ma, J.; Zhu, X.; Yarkony, D. R.; Xie, D.; Guo, H. Nonadiabatic Tunneling in Photodissociation of Phenol. *J. Am. Chem. Soc.* **2016**, *138*, 7828−7831.
(21) Ma, J.; Li, J.; Guo, H. Tunneling facilitated dissociation to H +CO2 in $HOCO^-$ photodetachment. *Phys. Rev. Lett.* **2012**, *109*, 063202.
(22) Schleif, T.; Merini, M. P.; Sander, W. The Mystery of the Benzene-Oxide/Oxepin Equilibrium-Heavy-Atom Tunneling Reversed by Solvent Interactions. *Angew. Chem., Int. Ed.* **2020**, *59*, 20318−20322.
(23) Henkel, S.; Merini, M. P.; Mendez-Vega, E.; Sander, W. Lewis acid catalyzed heavy atom tunneling - the case of 1H-bicyclo 3.1.0 -hexa-3,5-dien-2-one. *Chem. Sci.* **2021**, *12*, 11013−11019.
(24) Schleif, T.; Merini, M. P.; Henkel, S.; Sander, W. Solvation Effects on Quantum Tunneling Reactions. *Acc. Chem. Res.* **2022**, *55*, 2180−2190.
(25) Gonzalez-James, O. M.; Zhang, X.; Datta, A.; Hrovat, D. A.; Borden, W. T.; Singleton, D. A. Experimental evidence for heavy-atom tunneling in the ring-opening of cyclopropylcarbinyl radical from intramolecular $^{12}C/^{13}C$ kinetic isotope effects. *J. Am. Chem. Soc.* **2010**, *132*, 12548−12549.
(26) Ertelt, M.; Hrovat, D. A.; Borden, W. T.; Sander, W. Heavy-Atom Tunneling in the Ring Opening of a Strained Cyclopropene at Very Low Temperatures. *Chem. Eur. J.* **2014**, *20*, 4713−4720.
(27) Inui, H.; Sawada, K.; Oishi, S.; Ushida, K.; McMahon, R. J. Aryl nitrene rearrangements: Spectroscopic observation of a benzazirine and its ring expansion to a ketenimine by heavy-atom tunneling. *J. Am. Chem. Soc.* **2013**, *135*, 10246−10249.
(28) Chen, J.-L.; Hu, W.-P. Theoretical prediction on the thermal stability of cyclic ozone and strong oxygen tunneling. *J. Am. Chem. Soc.* **2011**, *133*, 16045−16053.
(29) Wu, Z.; Feng, R.; Li, H.; Xu, J.; Deng, G.; Abe, M.; Bégué, D.; Liu, K.; Zeng, X. Fast Heavy-Atom Tunneling in Trifluoroacetyl Nitrene. *Angew. Chem., Int. Ed.* **2017**, *56*, 15672−15676.
(30) Doubleday, C.; Armas, R.; Walker, D.; Cosgriff, C. V.; Greer, E. M. Heavy-Atom Tunneling Calculations in Thirteen Organic Reactions: Tunneling Contributions are Substantial, and Bell's Formula Closely Approximates Multidimensional Tunneling at≥ 250 K. *Angew. Chem., Int. Ed.* **2017**, *56*, 13099−13102.
(31) Michel, C. S.; Lampkin, P. P.; Shezaf, J. Z.; Moll, J. F.; Castro, C.; Karney, W. L. Tunneling by 16 carbons: planar bond shifting in [16] annulene. *J. Am. Chem. Soc.* **2019**, *141*, 5286−5293.

(32) Greer, E. M.; Cosgriff, C. V.; Doubleday, C. Computational evidence for heavy-atom tunneling in the Bergman cyclization of a 10-membered-ring enediyne. *J. Am. Chem. Soc.* **2013**, *135*, 10194−10197.
(33) Arbitman, J. K.; Michel, C. S.; Castro, C.; Karney, W. L. Calculations Predict That Heavy-Atom Tunneling Dominates Möbius Bond Shifting in [12]- and [16]Annulene. *Org. Lett.* **2019**, *21*, 8587−8591.
(34) Nunes, C. M.; Viegas, L. P.; Wood, S. A.; Roque, J. P. L.; McMahon, R. J.; Fausto, R. Heavy-Atom Tunneling Through Crossing Potential Energy Surfaces: Cyclization of a Triplet 2-Formylarylnitrene to a Singlet 2,1-Benzisoxazole. *Angew. Chem., Int. Ed.* **2020**, *59*, 17622−17627.
(35) Heller, E. R.; Richardson, J. O. Spin Crossover of Thiophosgene via Multidimensional Heavy-Atom Quantum Tunneling. *J. Am. Chem. Soc.* **2021**, *143*, 20952−20961.
(36) Greer, E. M.; Siev, V.; Segal, A.; Greer, A.; Doubleday, C. Computational Evidence for Tunneling and a Hidden Intermediate in the Biosynthesis of Tetrahydrocannabinol br. *J. Am. Chem. Soc.* **2022**, *144*, 7646−7656.
(37) Lin, C. F.; Durant, E.; Persson, M.; Rossi, M.; Kumagai, T. Real-Space Observation of Quantum Tunneling by a Carbon Atom: Flipping Reaction of Formaldehyde on Cu(110). *J. Phys. Chem. Lett.* **2019**, *10*, 645−649.
(38) Schleif, T.; Mieres-Perez, J.; Henkel, S.; Ertelt, M.; Borden, W. T.; Sander, W. The Cope Rearrangement of 1,5-Dimethylsemibullvalene-2(4)-d(1): Experimental Evidence for Heavy-Atom Tunneling. *Angew. Chem., Int. Ed.* **2017**, *56*, 10746−10749.
(39) Datta, A.; Hrovat, D. A.; Borden, W. T. Calculations predict rapid tunneling by carbon from the vibrational ground state in the ring opening of cyclopropylcarbinyl radical at cryogenic temperatures. *J. Am. Chem. Soc.* **2008**, *130*, 6684−6685.
(40) Viegas, L. P.; M. Nunes, C. M.; Fausto, R. Spin-forbidden heavy-atom tunneling in the ring-closure of triplet cyclopentane-1,3-diyl. *Phys. Chem. Chem. Phys.* **2021**, *23*, 5797−5803.
(41) Li, X.; Liao, T.; Chung, L. W. Computational prediction of excited-state carbon tunneling in the two steps of triplet zimmerman di-π-methane rearrangement. *J. Am. Chem. Soc.* **2017**, *139*, 16438−16441.
(42) Matute, R. A.; Houk, K. N. The Triplet Surface of the Zimmerman Di-π-Methane Rearrangement of Dibenzobarrelene. *Angew. Chem., Int. Ed.* **2012**, *51*, 13097−13100.
(43) Kuan, K. Y.; Singleton, D. A. Vibrationally Hot and Cold Triplets. Sensitizer-Dependent Dynamics and Localized Vibrational Promotion of a Di-π-methane Rearrangement. *J. Am. Chem. Soc.* **2020**, *142*, 19885−19888.
(44) Lan, J.; Li, X.; Yang, Y.; Zhang, X.; Chung, L. W. New Insights and Predictions into Complex Homogeneous Reactions Enabled by Computational Chemistry in Synergy with Experiments: Isotopes and Mechanisms. *Acc. Chem. Res.* **2022**, *55*, 1109−1123.
(45) Nunes, C. M.; Eckhardt, A. K.; Reva, I.; Fausto, R.; Schreiner, P. R. Competitive Nitrogen versus Carbon Tunneling. *J. Am. Chem. Soc.* **2019**, *141*, 14340−14348.
(46) Nunes, C. M.; Reva, I.; Kozuch, S.; McMahon, R. J.; Fausto, R. Photochemistry of 2-Formylphenylnitrene: A Doorway to Heavy-Atom Tunneling of a Benzazirine to a Cyclic Ketenimine. *J. Am. Chem. Soc.* **2017**, *139*, 17649−17659.
(47) Nandi, A.; Gerbig, D.; Schreiner, P. R.; Borden, W. T.; Kozuch, S. Isotope-Controlled Selectivity by Quantum Tunneling: Hydrogen Migration versus Ring Expansion in Cyclopropylmethylcarbenes. *J. Am. Chem. Soc.* **2017**, *139*, 9097−9099.
(48) Kozuch, S.; Zhang, X.; Hrovat, D. A.; Borden, W. T. Calculations on Tunneling in the Reactions of Noradamantyl Carbenes. *J. Am. Chem. Soc.* **2013**, *135*, 17274−17277.
(49) Fried, S. D.; Bagchi, S.; Boxer, S. G. Extreme electric fields power catalysis in the active site of ketosteroid isomerase. *Science* **2014**, *346*, 1510−1514.
(50) Ciampi, S.; Darwish, N.; Aitken, H. M.; Diez-Perez, I.; Coote, M. L. Harnessing electrostatic catalysis in single molecule, electrochemical and chemical systems: a rapidly growing experimental tool box. *Chem. Soc. Rev.* **2018**, *47*, 5146−5164.
(51) Geng, C.; Li, J. L.; Weiske, T.; Schlangen, M.; Shaik, S.; Schwarz, H. Electrostatic and Charge-Induced Methane Activation by a Concerted Double C-H Bond Insertion. *J. Am. Chem. Soc.* **2017**, *139*, 1684−1689.
(52) Aitken, H. M.; Coote, M. L. Can electrostatic catalysis of Diels-Alder reactions be harnessed with pH-switchable charged functional groups? *Phys. Chem. Chem. Phys.* **2018**, *20*, 10671−10676.
(53) Hirao, H.; Chen, H.; Carvajal, M. A.; Wang, Y.; Shaik, S. Effect of external electric fields on the C-H bond activation reactivity of Nonheme iron-oxo reagents. *J. Am. Chem. Soc.* **2008**, *130*, 3319−3327.
(54) Ramanan, R.; Danovich, D.; Mandal, D.; Shaik, S. Catalysis of Methyl Transfer Reactions by Oriented External Electric Fields: Are Gold-Thiolate Linkers Innocent? *J. Am. Chem. Soc.* **2018**, *140*, 4354−4362.
(55) Akamatsu, M.; Sakai, N.; Matile, S. Electric-Field-Assisted Anion-pi Catalysis. *J. Am. Chem. Soc.* **2017**, *139*, 6558−6561.
(56) Shaik, S.; Mandal, D.; Ramanan, R. Oriented electric fields as future smart reagents in chemistry. *Nat. Chem.* **2016**, *8*, 1091−1098.
(57) Shaik, S.; Ramanan, R.; Danovich, D.; Mandal, D. Structure and reactivity/selectivity control by oriented-external electric fields. *Chem. Soc. Rev.* **2018**, *47*, 5125−5145.
(58) Meir, R.; Chen, H.; Lai, W. Z.; Shaik, S. Oriented Electric Fields Accelerate Diels-Alder Reactions and Control the endo/exo Selectivity. *ChemPhysChem* **2010**, *11*, 301−310.
(59) Klinska, M.; Smith, L. M.; Gryn'ova, G.; Banwell, M. G.; Coote, M. L. Experimental demonstration of pH-dependent electrostatic catalysis of radical reactions. *Chem. Sci.* **2015**, *6*, 5623−5627.
(60) Aragones, A. C.; Haworth, N. L.; Darwish, N.; Ciampi, S.; Bloomfield, N. J.; Wallace, G. G.; Diez-Perez, I.; Coote, M. L. Electrostatic catalysis of a Diels-Alder reaction. *Nature* **2016**, *531*, 88−91.
(61) Gorin, C. F.; Beh, E. S.; Bui, Q. M.; Dick, G. R.; Kanan, M. W. Interfacial Electric Field Effects on a Carbene Reaction Catalyzed by Rh Porphyrins. *J. Am. Chem. Soc.* **2013**, *135*, 11257−11265.
(62) Park, Y.; Kang, H.; Field, R. W.; Kang, H. The frequency-domain infrared spectrum of ammonia encodes changes in molecular dynamics caused by a DC electric field. *Proc. Natl. Acad. Sci. U. S. A.* **2019**, *116*, 23444−23447.
(63) Kirshenboim, O.; Frenklah, A.; Kozuch, S. Switch chemistry at cryogenic conditions: quantum tunnelling under electric fields. *Chem. Sci.* **2021**, *12*, 3179−3187.
(64) Álvarez-Barcia, S.; Flores, J. R.; Kästner, J. Tunneling Above the Crossover Temperature. *J. Phys. Chem. A* **2014**, *118*, 78−82.
(65) This site-selectivity of the arene molecule containing two hydroxycarbene groups can be mainly ascribed to the larger difference in the energy barriers (2.1 kcal/mol for R_D and 1.2 kcal/mol for R_E).
(66) Zhou, Y. N.; Li, J. J.; Wu, Y. Y.; Luo, Z. H. Role of External Field in Polymerization: Mechanism and Kinetics. *Chem. Rev.* **2020**, *120*, 2950−3048.

https://doi.org/10.1021/acs.jpclett.2c03461
J. Phys. Chem. Lett. 2023, 14, 1124−1132